Check for updates

Orientation-controllable growth of Co₃O₄ single nanocrystals using a BiCoO₃ target by pulsed laser deposition

Deyang Chen, [ID] *[ab] Shang-Lin Hsu,[b] Ajay K. Yadav [ID] [b] and James D. Clarkson[b]

We report a novel route to synthesize Co₃O₄ single nanocrystals using pulsed laser deposition by decomposition of BiCoO₃. The decomposition of BiCoO₃ to Bi₂O₃ and Co₃O₄ at relatively high temperature enables the formation of pure Co₃O₄ phase. The absence of Bi element is confirmed by both X-ray diffraction (XRD) and energy dispersive spectrometer (EDS) measurements. The effects of various PLD growth conditions, including growth rate (2–20 Hz), growth temperature (630–650 °C), O₂ partial pressure (50–200 mTorr) and laser energy density (0.6–1.8 J cm⁻²), on the synthesis of Co₃O₄ nanocrystals were systematically studied. Interestingly, the orientation of Co₃O₄ single nanocrystals can be controlled by changing the growth parameters. It is revealed that the decrease of the laser energy density leads to the preferred orientation of Co₃O₄ single nanocrystals altering from (111) plane to (220), while the high temperature growth favors (400) orientation. The obtained orientation-controllable Co₃O₄ single nanocrystals provide the possibility to study its orientation-dependent physical and chemical properties as catalysts, anode materials and magnetic materials.

Introduction

Co₃O₄ is attracting much attention for its thermodynamic stability, electrochemical properties and antiferromagnetic properties, promising for catalyst, Li-ion battery, gas sensor and spintronic device applications.[1–6] Both the experimental and theoretical studies have revealed that the crystallographic orientation and morphology of the metallic oxides play a key role in the related physical and chemical properties as different orientations or morphologies not only have various surface atomic densities but also electronic structures.[7–11] Hu *et al.*[12] found significant effects of crystal orientation in Co₃O₄ on catalytic properties. It was also demonstrated that the exposed facets of Co₃O₄ nanocrystals play an important role in Li-ion battery.[13] Moreover, Yu *et al.*[14] reported that the electrochemical sensing performance in (111) facet of Co₃O₄ nanoplates is better than that of the (001) facet of Co₃O₄ nanocubes.

Thereby, much effort has been made to synthesize various oriented single nanocrystals (such as nanoparticles, nanowires and nanosheets) by chemical solution deposition method, magnetron sputtering, pulsed laser deposition, post calcination, thermal evaporation, wet chemical synthetic approach, and so on.[15–21] However, a synthesis method to produce orientation-controllable and morphology-tunable Co₃O₄ single nanocrystals is extremely desirable as it could provide a platform for the study of orientation-dependent and morphology-related catalytic, magnetic and electrochemical properties where enhanced physical or chemical properties may be obtained for promising applications.

In this study, a novel route is proposed to synthesize Co₃O₄ single nanocrystals using a BiCoO₃ target by pulsed laser deposition (PLD). We would like to mention that the term of "single nanocrystals" here presents the epitaxial grew Co₃O₄ nanoparticles. We show that the orientations of the Co₃O₄ can be well-controlled by change the PLD growth parameters (such as growth rate, growth temperature, O₂ partial pressure and laser energy density). The decomposition of BiCoO₃ to Bi₂O₃ and Co₃O₄ at relatively high temperature (630 °C) enables the formation of pure Co₃O₄ phase. The absence of Bi element is confirmed by both X-ray diffraction (XRD) and energy dispersive spectrometer (EDS) measurements. We systematically studied the effects of various PLD growth conditions, including growth rate (2–20 Hz), growth temperature (630–650 °C), O₂ partial pressure (50–200 mTorr) and laser energy density (0.6–1.8 J cm⁻²), on the synthesis of Co₃O₄ nanocrystals.

By changing different growth parameters, (111), (220) and (400) orientation-controlled Co₃O₄ single nanocrystals have been obtained. It turns out that (111) oriented Co₃O₄ single nanocrystals can be synthesized at slower growth rate and lower O₂ partial pressure, while lower growth temperature and higher O₂ partial pressure result in the formation of the (111) oriented Bi₂O₃ impurity. More interestingly, it is

a Institute for Advanced Materials (IAM), South China Normal University, Guangzhou 510006, China. E-mail: dychen1987@gmail.com

b Department of Materials Science and Engineering, University of California, Berkeley, California 94720, USA

revealed that the decrease of the laser energy density leads to the preferred orientation of Co_3O_4 single nanocrystals altering from (111) plane to (220). Furthermore, we found that higher growth temperature would give rise to the synthesis of (400) oriented Co_3O_4 single nanocrystals. These findings provide a novel approach to prepare the orientation-controllable Co_3O_4 single nanocrystals, which offer a possibility to study the orientation-related properties of Co_3O_4 for potential applications in catalysts, anode materials and magnetic materials.

Experimental

Sample preparation

A series of Co_3O_4 samples were grown using a $BiCoO_3$ target on (110) $YAlO_3$ substrates by pulsed laser deposition (PLD) using a KrF excimer laser ($\lambda = 248$ nm) in various growth conditions with growth rate at 2–20 Hz, growth temperature from 630 to 650 °C, O_2 partial pressure of 50–200 mTorr and laser energy density at 0.6–1.8 J cm^{-2}.

Characterizations

A combination of X-ray diffraction (XRD, PANalytical X'Pert) and transmission electron microscopy (TEM, Titan X 200 kV) were used for the structural characterization. The composition of the obtained samples were measured by energy dispersive spectrometer (EDS). Atomic force microscopy (AFM, Veeco, Multi-Mode 8) was applied to study the morphologies of Co_3O_4 nanocrystals.

Results and discussion

A variety of parameters play important roles in the PLD growth process. Among of these conditions, the growth rate, growth temperature, O_2 partial pressure and laser energy density are critical to obtain high quality samples.[22,23] In this work, we first study the effects of growth rates (2–20 Hz) on the synthesis of Co_3O_4 single nanocrystals as shown in Fig. 1. The Co_3O_4 was grown by pulsed laser deposition (PLD) at various pulsed laser frequencies (2, 10 and 20 Hz) with the laser energy density of 1.1 J cm^{-2} at 630 °C in an oxygen pressure of 100 mTorr. At the growth temperature ∼630 °C (much higher than the decomposition temperature of $BiCoO_3$), $BiCoO_3$ would decompose to Bi_2O_3 and Co_3O_4.[24] This is verified by the XRD measurement (Fig. 1a) and provides a possibility to obtain pure Co_3O_4 phase by adjusting the growth parameters. The XRD data show that (111) oriented single crystal Co_3O_4 with (111) Bi_2O_3 impurity were synthesized at low growth rate (2 Hz), while (111), (311) and (400) polycrystalline Co_3O_4 were obtained with the increase of the growth rate to 10 Hz. The poly-crystallization of Co_3O_4 were even promoted with the (220) diffraction peak emerging at 20 Hz. It is also worth to note that the amount of Bi_2O_3 secondary phase increases at higher growth rate (10 Hz and 20 Hz) as shown in Fig. 1a. This is because the high growth rate hinders the volatilization of Bi element, whereas the low growth rate of 2 Hz helps its volatilization to obtain pure phase Co_3O_4. The morphologies of the samples grown at 2 Hz, 10 Hz and 20 Hz were captured by atomic force microscopy (AFM) as shown in Fig. 1b–d, respectively. The triangle-like morphology presented in Fig. 1b points to the (111) oriented growth of Co_3O_4 nanocrystals, which is in agreement with the XRD data. This is
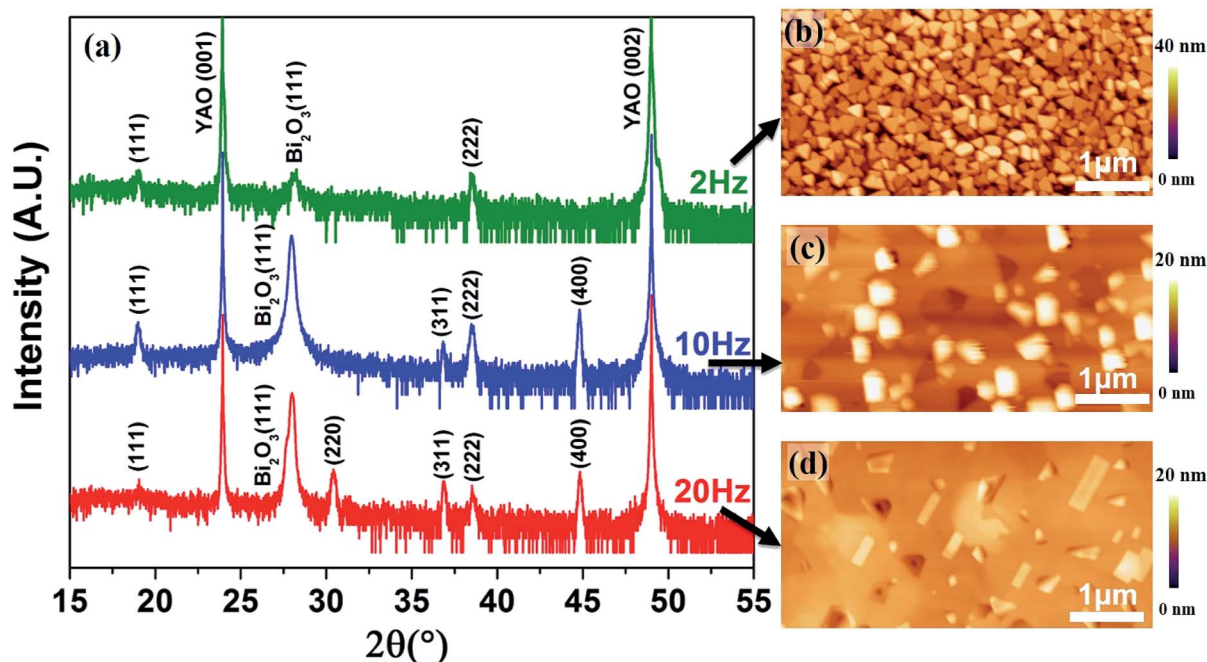

Fig. 1 The effects of growth rate on the synthesis of Co_3O_4 single nanocrystals. (a) XRD data of Co_3O_4 samples grown at various growth rate (2 Hz, 10 Hz and 20 Hz). AFM topography images showing the morphologies of the corresponding samples: (b) 2 Hz, (c) 10 Hz and (d) 20 Hz.

also consistent with previous study.[25] Nevertheless, the poly-crystalline Co_3O_4 samples synthesized at 10 Hz and 20 Hz show particles with various shapes embedded in continuous films (Fig. 1c and d). These results indicate that pure phase, (111) oriented Co_3O_4 single nanocrystal favors low growth rate.

The influences of growth temperature on the preparation of Co_3O_4 were also studied as shown in Fig. 2. The Co_3O_4 samples were grown at 10 Hz with the laser energy density of 1.1 J cm^{-2}
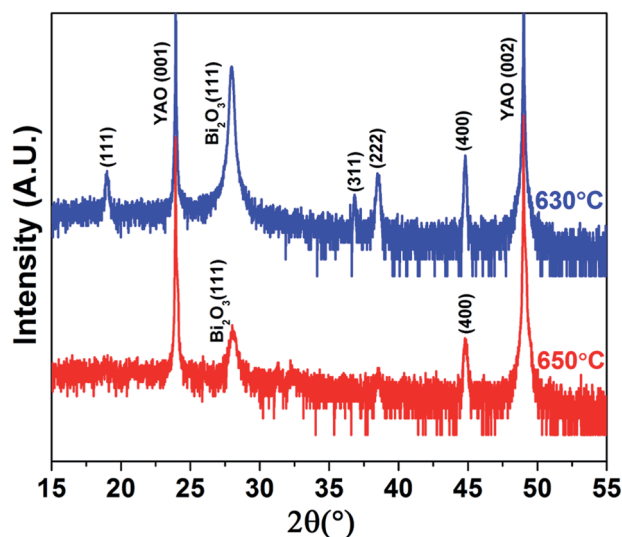

Fig. 2   Effects of growth temperate (630–650 °C) on the synthesis of Co_3O_4 single nanocrystals, revealing the preferred (400) oriented growth of Co_3O_4 in higher temperature (650 °C).

in an oxygen pressure of 100 mTorr at 630–650 °C. The XRD data demonstrate that high growth temperature contributes to the growth of (400) oriented Co_3O_4. However, there is the impurity Bi_2O_3 phase in all these samples grown at different growth rates and temperatures.

As the secondary Bi_2O_3 phase is sensitive to the O_2 partial pressure as well,[26,27] to obtain pure Co_3O_4, we next focus on the effects of this growth parameter. The samples were grown at 2 Hz with 1.1 J cm^{-2} energy density at 630 °C in the O_2 pressure of 50–200 mTorr. XRD was performed for the structural characterization. As expected, the O_2 pressure has significant effects on the formation of the Bi_2O_3 impurity. With the decrease of the O_2 pressure from 200 mTorr to 100 mTorr, the content of Bi_2O_3 reduced significantly and pure (111) oriented Co_3O_4 was successfully obtained with the further decrease of O_2 to 50 mTorr, as displayed in Fig. 3a. All the corresponding AFM topography images (Fig. 3b–d) show similar triangle-like morphologies in agreement with the XRD data (Fig. 3a) and the growth rate dependent study (Fig. 1), further indicating the (111) oriented growth of Co_3O_4 single nanocrystals. The size of the obtained Co_3O_4 single nanocrystals are 100–350 nm. We would like to mention that both the Co_3O_4 and Bi_2O_3 are (111)-oriented single nanocrystals, thus it is difficult to tell the difference in the topography images as they both show triangle-like morphology.

The laser energy density is another important growth parameter of PLD, which would affect the formation of the desired phase and the impurities.[28] Interestingly, we find that this growth parameter can be used to control the orientation of Co_3O_4 nanocrystals. Three samples were grown with different
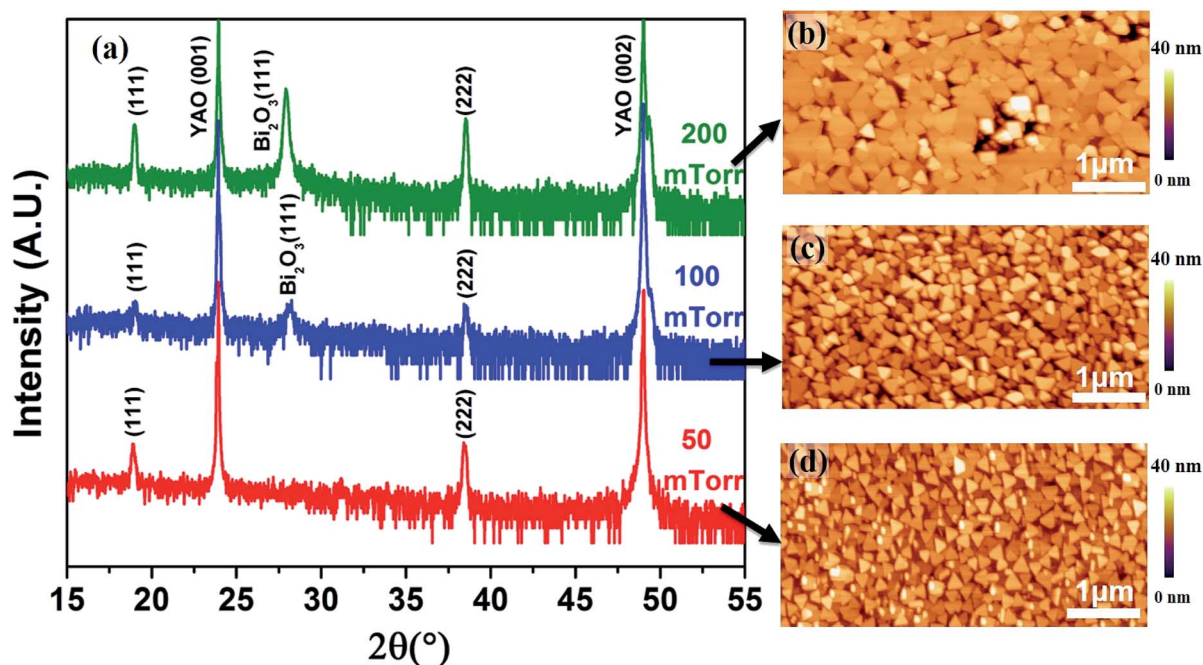

Fig. 3   Effects of oxygen partial pressure on the synthesis of Co_3O_4 single nanocrystals. (a) XRD data of Co_3O_4 samples grown at different O_2 pressure (50–200 mTorr). AFM topography images showing the morphologies of the corresponding samples: (b) 200 mTorr, (c) 100 mTorr and (d) 50 mTorr.

laser energy density (0.6–1.8 J cm^{-2}) while other growth parameters were the same (50 mTorr, 2 Hz, 630 °C). As shown in Fig. 4a, it is revealed that high energy density (1.8 J cm^{-2}) leads to the formation of (111) and (220) mixed orientation of Co$_3$O$_4$ nanocrystals. (111) Single nanocrystal Co$_3$O$_4$ were synthesized with the reduction of energy density to 1.1 J cm^{-2}, whereas the preferred orientation alters to (220) plane with even lower energy density of 0.6 J cm^{-2}.

Meanwhile, the corresponding morphologies are very different as shown in the AFM images (Fig. 4b–d). The (111) and (220) mixed orientation samples obtained at 1.8 J cm^{-2} show irregular shapes (Fig. 4b) whereas the (111) oriented Co$_3$O$_4$ single nanocrystals grown at 1.1–1.8 J cm^{-2} possess triangle-like morphology (Fig. 4c), again in consistent with the grow rate and oxygen pressure dependent studies (Fig. 1 and 3). Differently, when the orientation of Co$_3$O$_4$ change to (220) plane with the decrease of energy density to 0.6 J cm^{-2}, it shows sandwich-like morphology as shown in Fig. 4d. The typical sandwich-like Co$_3$O$_4$ nanocrystals are marked with blue squares while triangle-like nanocrystals marked with white circles are also observed, indicating the existence of a small amount of (111) oriented Co$_3$O$_4$ which was not detected by XRD. These findings are promising for the study of the morphology-dependent and orientation-dependent catalytic, magnetic and electrochemical properties.

To further study the structure and composition of the obtained Co$_3$O$_4$ single nanocrystals, transmission electron microscopy (TEM), Scanning TEM (STEM) and energy dispersive spectrometer (EDS) were performed on a (111) oriented Co$_3$O$_4$ sample as shown in Fig. 4c at the National Center for Electron

Microscopy (NCEM), Lawrence Berkeley National Laboratory (LBNL). Fig. 5a shows the high-angle annular dark field (HAADF) low-resolution STEM image of Co$_3$O$_4$ sample grown on YAlO$_3$ substrate. The EDS elemental line scan profile is shown in Fig. 5b, which was conducted across a Co$_3$O$_4$ nanocrystal along the red line as shown in Fig. 5a. The corresponding EDS line scan across HAADF STEM image is presented in Fig. 5c. It reveal the existence of Co and O in the layer of Co$_3$O$_4$ nanocrystal and the presence of Y, Al and O in the layer of YAlO$_3$ substrate, while the Bi element from the BiCoO$_3$ target is absent due to its decomposition during the growth process. This is in agreement of our XRD data. The EDS elemental mappings of Bi, Co and O elements corresponding to the HAADF STEM image in Fig. 5a were measured as well as shown in Fig. 5d–f. It again demonstrate the absence of Bi (as shown in Fig. 5d, the discontinuous blue contrast is the background signal). Fig. 5e shows that the Co element only exists in the Co$_3$O$_4$ single nanocrystals layer while Fig. 5f reveals that oxygen exists across the whole sample. Thus, these results demonstrate the pure Co$_3$O$_4$ phase has been obtained in this study.

A low-resolution cross sectional TEM image of the (111) oriented Co$_3$O$_4$ sample (as shown in Fig. 4c) is presented in Fig. 6a. It shows that the discontinuous Co$_3$O$_4$ nanocrystals with size around 100–250 nm are synthesized on YAlO$_3$ substrate. The high-resolution TEM image of the red circled region in Fig. 6a is shown in Fig. 6b. The green dashed line reveals the sharp interface between the Co$_3$O$_4$ layer and YAlO$_3$ substrate. Moreover, the lattice spacing of 4.67 Å verifies the (111) oriented growth of Co$_3$O$_4$ single nanocrystals, which is again in agreement with the previous data (Fig. 4).
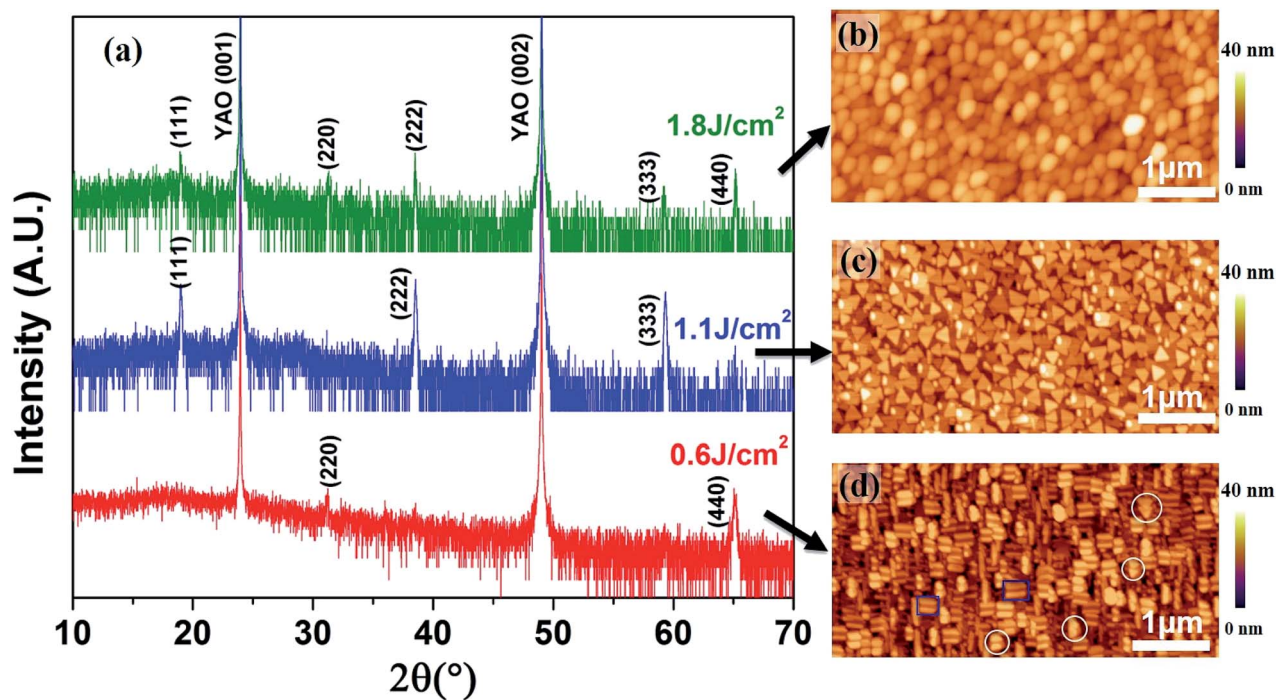

Fig. 4 Effects of laser energy density on the synthesis of Co$_3$O$_4$ single nanocrystals. (a) XRD data of Co$_3$O$_4$ samples grown at different energy density (0.6–1.8 J cm^{-2}). AFM topography images showing the morphologies of the corresponding samples: (b) 1.8 J cm^{-2}, (c) 1.1 J cm^{-2}, and (d) 0.6 J cm^{-2}.
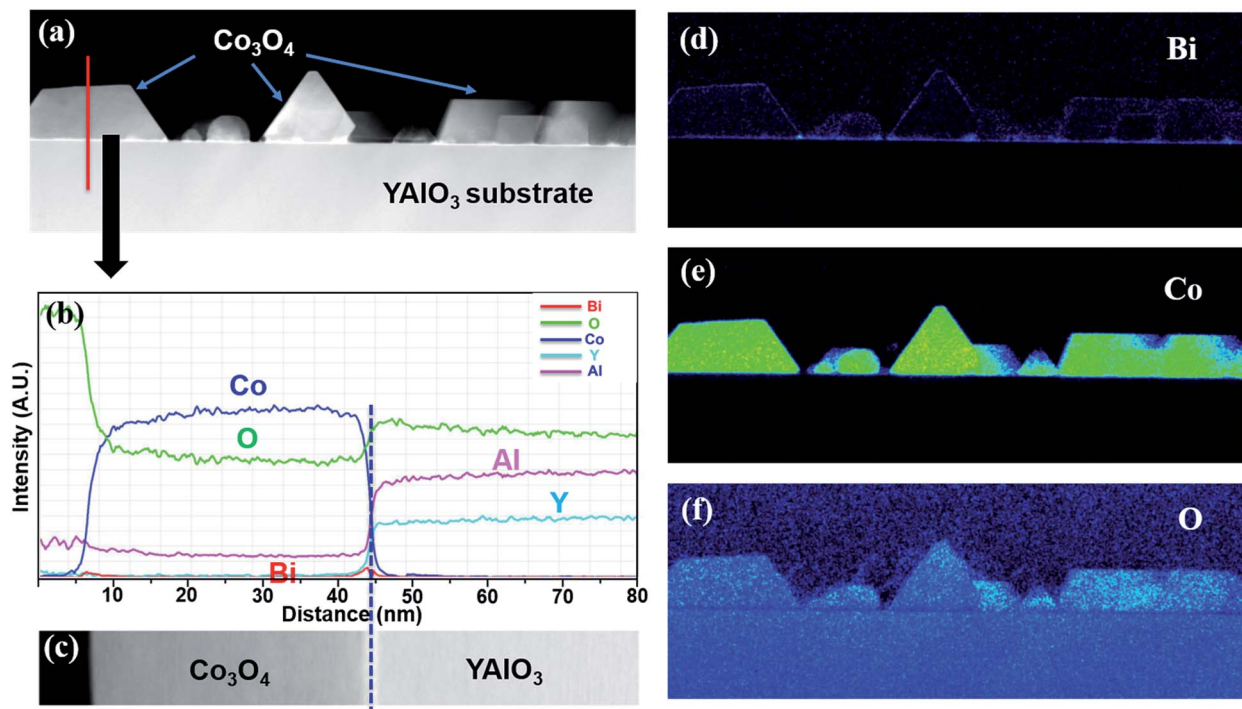
Fig. 5 (a) Low-resolution HAADF STEM image of Co_3O_4 sample grown on $YAlO_3$ substrate. (b) EDS elemental line scan profile across the red line in (a). (c) The HAADF STEM image of the region conducted with EDS line scan. The EDS elemental mappings of Bi, Co and O elements corresponding to the HAADF STEM image in (a): (d) Bi element, (e) Co element, and (f) O element.
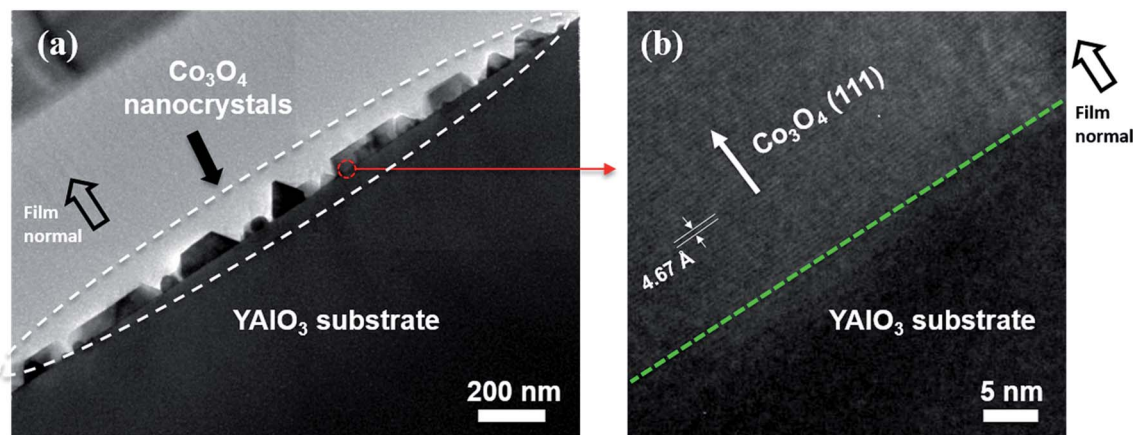

Fig. 6 (a) A low-resolution cross sectional TEM image of the (111) oriented Co_3O_4 sample. (b) The high-resolution TEM image of the red circled region in (a). The green dashed line reveals the sharp interface between the Co_3O_4 layer and $YAlO_3$ substrate. The lattice spacing of 4.67 Å verifies the (111) oriented growth of Co_3O_4 single nanocrystals.

Conclusions

To summarize, we report a novel approach to synthesize single nanocrystal Co_3O_4 using PLD by the decomposition of $BiCoO_3$. The absence of Bi element owing to the decomposition of $BiCoO_3$ during the growth process is verified by both X-ray diffraction (XRD) and energy dispersive spectrometer (EDS) measurements. We show that the orientation of Co_3O_4 can be well-controlled by changing the PLD growth conditions. (111), (220) and (400) oriented Co_3O_4 single nanocrystals have been

successfully obtained. It is revealed that the decrease of the laser energy density leads to the preferred orientation of Co_3O_4 single nanocrystals altering from (111) plane to (220), while the high temperature growth favors (400) orientation. Moreover, distinct morphologies of different orientation Co_3O_4 single nanocrystals are observed by AFM. The (111) oriented growth samples show triangle-like morphology while the (220) samples display sandwich-like topography. These findings offer a new route to obtain orientation-controllable Co_3O_4 single nanocrystals and provide the possibility to study the orientation-

dependent and morphology-dependent physical and chemical properties of Co_3O_4 as catalysts, anode materials and magnetic materials. Furthermore, the decomposition of $BiCoO_3$ in high temperature (630–650 °C) in this study also might give a clue to grow $BiCoO_3$ thin films, which is a superior room temperature ferroelectric material,[29] in relatively low temperature.

Conflicts of interest

There are no conflicts to declare.

Acknowledgements

References

1 A. Alvarez, S. Ivanova, M. A. Centeno and J. A. Odriozola, *Appl. Catal., A*, 2012, **431**, 9–17.
2 R. Gao, J. Z. Zhu, X. L. Xiao, Z. B. Hu, J. J. Liu and X. F. Liu, *J. Phys. Chem. C*, 2015, **119**, 4516–4523.
3 K. B. Yin, J. Ji, Y. T. Shen, Y. W. Xiong, H. C. Bi, J. Sun, T. Xu, Z. Y. Zhu and L. T. Sun, *J. Alloys Compd.*, 2017, **720**, 345–351.
4 J. M. Xu and J. P. Cheng, *J. Alloys Compd.*, 2016, **686**, 753–768.
5 B. L. Ellis, P. Knauth and T. Djenizian, *Adv. Mater.*, 2014, **26**, 3368–3398.
6 W. Wei, Z. Wang, Z. Liu, Y. Liu, L. He, D. Chen, A. Umar, L. Guo and J. Li, *J. Power Sources*, 2013, **238**, 376–387.
7 Y. Gong, F. Gong, C. Wang, H. Zheng and F. Li, *RSC Adv.*, 2015, **5**, 27266–27272.
8 Z. L. Wang, *J. Phys. Chem. B*, 2000, **104**, 1153–1175.
9 T. Ouyang, K. Cheng, S. Kong, K. Ye, Y. Gao, D. Zhang, G. Wang and D. Cao, *RSC Adv.*, 2015, **5**, 36059–36065.
10 X. Xie, Y. Li, Z.-Q. Liu, M. Haruta and W. Shen, *Nature*, 2009, **458**, 746–749.
11 L. Jin, X. Li, H. Ming, H. Wang, Z. Jia, Y. Fu, J. Adkins, Q. Zhou and J. Zheng, *RSC Adv.*, 2014, **4**, 6083–6089.
12 L. H. Hu, Q. Peng and Y. D. Li, *J. Am. Chem. Soc.*, 2008, **130**, 16136–16137.
13 X. Xiao, X. Liu, H. Zhao, D. Chen, F. Liu, J. Xiang, Z. Hu and Y. Li, *Adv. Mater.*, 2012, **24**, 5762–5766.
14 X. Y. Yu, Q. Q. Meng, T. Luo, Y. Jia, B. Sun, Q. X. Li, J. H. Liu and X. J. Huang, *Sci. Rep.*, 2013, **3**, 2886.
15 Z. Dong, Y. Y. Fu, Q. Han, Y. Y. Xu and H. Zhang, *J. Phys. Chem. C*, 2007, **111**, 18475–18478.
16 L. F. Chen, J. C. Hu, R. Richards, S. Prikhodko and S. Kodambaka, *Nanoscale*, 2010, **2**, 1657–1660.
17 J. Bursik, M. Soroka, R. Uhrecky, R. Kuzel, F. Mika and S. Huber, *Appl. Surf. Sci.*, 2016, **376**, 209–218.
18 J. Lu, S. Cheng, M. Liu and C. Jia, *CrystEngComm*, 2016, **18**, 8038–8043.
19 A. Matsuda, R. Yamauchi, D. Shiojiri, G. Tan, S. Kaneko and M. Yoshimoto, *Appl. Surf. Sci.*, 2015, **349**, 78–82.
20 J.-M. Li, *CrystEngComm*, 2017, **19**, 3392–3397.
21 J.-M. Li, *Cryst. Growth Des.*, 2009, **9**, 4171–4175.
22 M. N. R. Ashfold, F. Claeyssens, G. M. Fuge and S. J. Henley, *Chem. Soc. Rev.*, 2004, **33**, 23–31.
23 H. M. Christen and G. Eres, *J. Phys.: Condens. Matter*, 2008, **20**, 264005.
24 A. A. Belik, S. Iikubo, K. Kodama, N. Igawa, S. Shamoto, S. Niitaka, M. Azuma, Y. Shimakawa, M. Takano, F. Izumi and E. Takayama-Muromachi, *Chem. Mater.*, 2006, **18**, 798–803.
25 L. Qiao, H. Y. Xiao, H. M. Meyer, J. N. Sun, C. M. Rouleau, A. A. Puretzky, D. B. Geohegan, I. N. Ivanov, M. Yoon, W. J. Weber and M. D. Biegalski, *J. Mater. Chem. C*, 2013, **1**, 4628–4633.
26 H. Bea, M. Bibes, A. Barthelemy, K. Bouzehouane, E. Jacquet, A. Khodan, J. P. Contour, S. Fusil, F. Wyczisk, A. Forget, D. Lebeugle, D. Colson and M. Viret, *Appl. Phys. Lett.*, 2005, **87**, 072508.
27 S. Fujino, M. Murakami, S. H. Lim, M. Wuttig, L. G. Salamanca-Riba and I. Takeuchi, *Solid State Ionics*, 2007, **178**, 1257–1261.
28 L. W. Martin, Y. H. Chu and R. Ramesh, *Mater. Sci. Eng., R*, 2010, **68**, 89–133.
29 Y. Uratani, T. Shishidou, F. Ishii and T. Oguchi, *Jpn. J. Appl. Phys.*, 2005, **44**(Part 1), 7130–7133.